AD-A120 067 CALIFORNIA UNIV LOS ANGELES DEPT OF MATERIALS SCIEN--ETC F/G 11/6
EFFECTS OF HEAT-TREATMENT ON PRE-YIELD BURST EMISSIONS OF A533B--ETC(U)
SEP 82 H TEOH, I ROMAN, K ONO N00014-81-K-0011
UNCLASSIFIED TR-82-01 NL

END
DATE FILMED
11-82
DTIC

SECURITY CLASSIFICATION OF THIS PAGE (When Data Entered)

12

REPORT DOCUMENTATION PAGE	READ INSTRUCTIONS BEFORE COMPLETING FORM
1. REPORT NUMBER: TR-82-01	2. GOVT ACCESSION NO.: AD-A120 067
3. RECIPIENT'S CATALOG NUMBER	
4. TITLE (and Subtitle): Effects of Heat-Treatment on Pre-yield Burst Emissions of A533B Steel	5. TYPE OF REPORT & PERIOD COVERED: Technical
	6. PERFORMING ORG. REPORT NUMBER
7. AUTHOR(s): H.B. Teoh, I. Roman and Kanji Ono	8. CONTRACT OR GRANT NUMBER(s): N00014-81-K-0011
9. PERFORMING ORGANIZATION NAME AND ADDRESS: University of California, Los Angeles, California 90024	10. PROGRAM ELEMENT, PROJECT, TASK AREA & WORK UNIT NUMBERS
11. CONTROLLING OFFICE NAME AND ADDRESS: Physics Program, Physical Sciences Div. Office of Naval Research Arlington, Virginia 22217	12. REPORT DATE: September, 1982 13. NUMBER OF PAGES: 10
14. MONITORING AGENCY NAME & ADDRESS (if different from Controlling Office): Office of Naval Research Branch Office 1030 East Green Street Pasadena, California 91101	15. SECURITY CLASS. (of this report): Unclassified 15a. DECLASSIFICATION/DOWNGRADING SCHEDULE

16. DISTRIBUTION STATEMENT (of this Report)

Approved for public release, distribution unlimited

17. DISTRIBUTION STATEMENT (of the abstract entered in Block 20, if different from Report)

18. SUPPLEMENTARY NOTES

To be published in The Proceedings of the 6th International Acoustic Emission Symposium, Susono City, Japan, 31 October - 3 November 1982.

19. KEY WORDS (Continue on reverse side if necessary and identify by block number)

Acoustic Emission
Structural Steels (A533B)
Plastic Deformation
Fracture
Non-metallic Inclusions
Heat Treatment of Steel

20. ABSTRACT (Continue on reverse side if necessary and identify by block number)

SEE NEXT PAGE

DD FORM 1 JAN 73 1473 EDITION OF 1 NOV 65 IS OBSOLETE
S/N 0102-LF-014-6601

EFFECTS OF HEAT-TREATMENT ON PRE-YIELD BURST EMISSIONS OF A533B STEEL

Hong-Bee Teoh, Itzhak Roman*, and Kanji Ono
Department of Materials Science and Engineering
School of Engineering and Applied Science
University of California
Los Angeles, California 90024

*Permanent address: Hebrew University, Jerusalem, Israel

ABSTRACT

Nonmetallic inclusions strongly affect the ductility and acoustic emission (AE) characteristics of A533B steel. Our present and previous studies have revealed highly anisotropic AE behavior during tensile and fracture testing, originating from the particular morphological features of MnS inclusions.

In the present study, the effect of different heat-treatment practices on the role of MnS-matrix interfaces in generating AE has been investigated. Although both L and S orientations of ASTM A533B steel were examined, pre-yield, burst-type emissions were observed only in the S-orientation.

The pre-yield, burst type AE activities increased drastically with tempering temperature (up to 750°C) for samples that were furnace-cooled after tempering. A maximum in this AE activity was noted, for specimens that were oil-quenched subsequent to tempering, around a tempering temperature of 600°C.

This AE behavior is explained by the occurrence of two phenomena. First, some of the MnS-matrix interfaces debond due to thermal stresses set up during quenching. Second, during tempering, partial cohesion of debonded interfaces commences along with the segregation of sulfur to the interfaces. Upon tensile loading, these interfaces fracture at relatively low stresses and generate the observed, burst-type AE in the pre-yield region of the S-orientation tensile samples.

INTRODUCTION

Acoustic Emission (AE) from ductile structural steels primarily originates from dislocation processes and nonmetallic inclusions. These produce continuous-type and burst-type emissions, respectively. See references 1 and 2 for a comprehensive listing of previous studies. Our previous studies on burst emissions have revealed that the decohesion of manganese sulfide (MnS) inclusions is the cause of strong influence of sulfur content on highly anisotropic fracture toughness and AE behavior (2-7). We further assert that most burst emissions detected during the loading of a ductile steel member are produced by the decohesion and fracture of nonmetallic inclusions.

It is well known that the ductility and fracture toughness of structural steels are strongly affected by heat-treatment and cleanliness, i.e., the presence of nonmetallic inclusions such as MnS. In order to evaluate the role of the inclusions, AE techniques are ideally suited to determine the conditions when the decohesion of the inclusions occurs. While no previous

work on steels exists, we anticipate effects of heat treatment on the strength and adhesion of inclusion-matrix interfaces to be significant. Roman and Jinchuk (8) have noted that sintered tungsten alloys exhibit varied toughness depending on heat treatment, attributable to the strength of the tungsten-matrix interfaces.

In this study, we varied heat treatment conditions on A533B steel tensile specimens in the longitudinal (L) and short-transverse (S) directions. Subsequently, the samples were tested in tension and the AE characteristics evaluated. As expected, drastic variations in pre-yield, burst-type AE were observed. The results indicate the debonding of the MnS-matrix interfaces upon quenching, the restoration of the interfacial bonds via mechanical and diffusion processes, and subsequent debonding upon loading. Thermal stresses appear to be the primary driving force for the observed phenomenon. The impurity segregation to interfaces also contributes to the observed behavior. This interpretation is consistent with the chemical composition at the interfaces (9) and the lattice parameter measurements of MnS using X-ray diffraction (10).

MATERIAL AND EXPERIMENTAL PROCEDURES

A 165 mm thick low sulfur plate supplied by Nippon Steel Corporation was the starting stock. Its chemical composition was given in reference 2. Sample geometry and test procedures were also identical to those used earlier (1,2). The tensile specimens were austenitized at 930°C for 1 hour in vacuum and subsequently quenched into oil at ambient temperature. Most of the specimens were tempered prior to testing and two tempering practices were employed. Some of the specimens were tempered at temperatures in the range of 150°C to 750°C for 24 hours. The rest of the specimens were tempered at 450°C, 550°C or 650°C for periods of time ranging from 5 to 14400 minutes. All samples (except a few noted as slow-cooled) were oil quenched after tempering.

AE characteristics evaluated were totalized AE event counts, rms voltages and the peak amplitude distribution of AE signals. A resonant type transducer (Model AC 175L, Acoustic Emission Technology Corporation [AET], Sacramento, California) and a preamplifier with 125-250 kHz filter (Model 160, AET) were used for all AE measurements. The transducer was acoustically coupled to the end of the round tensile samples using a viscous resin. For the AE event count measurements and the amplitude distribution analysis, a microcomputer based AE instrumentation (Model 5000, AET) and an amplitude distribution analyzer (Model 203, AET) were employed. A true rms voltmeter (Model 3400A, Hewlett-Packard) was used for the rms voltage measurements. The input noise level was 1.4 μV and the threshold for amplitude distribution analyzer was set at 15 mV after 60 dB amplification (or 15 μV in reference to the preamplifier input).

RESULTS

The yield and tensile strength of oil-quenched and tempered samples decreased with tempering temperature. The strength levels were lower than those of the water-quenched and tempered samples (1), but the general trends were quite similar. The S-orientation samples had slightly lower strengths, possibly reflecting the differences in texture. Elongation, reduction in area and true fracture stress were substantially lower in the S-orientation, but tempering at temperatures above 500°C removed the orientation effects on ductility. Continuous yielding was observed after tempering below 600°C. After 650°C tempering, a yield drop and Lueders strain were observed.

The observed AE behavior of the L-orientation samples was essentially identical to that of the water-quenched and tempered samples of the transverse orientation, reported by Landy and Ono (1). The load vs. time and rms voltage of AE signals vs. time curves for an oil-quenched sample are shown in Fig. 1. The total elongation is 15%, and time of 1 min. approximately corresponds to 7% plastic strain beyond yield. Continuous-type AE was observed almost from the beginning of macroscopically elastic deformation. The rms voltage increased gradually, reaching a broad maximum at about 80% of the yield load. Even at the maximum, the AE level was low (2.4μV), and decreased with further work-hardening to the background level. Spikes in the rms voltage-time curve represent occasional burst emissions, which totaled less than 500 for the entire test up to the maximum load.

Moderate tempering (250°C - 500°C) increased the level of near-yield continuous emission to very high values (55 to 90μV at the peak). The rms voltage-time curves were sharpened and higher stresses (70 to 90% of the yield) were required before any AE activities were detected. Again, continuous emission was primarily observed. Although the high signal levels resulted in large numbers of event counts, these were due to large excursions in the continuous-type signals. Tempering at 550°C to 700°C reduced the peak AE levels to 5 to 20μV range and further sharpened the rms voltage-time curve. When Lueders deformation was observed, AE intensity showed a double peak behavior, which became very low once the work-hardening started.

The AE behavior of the as-quenched sample of the S-orientation was identical to that of the L-orientation, even though the ductility indicators were lower in the S-sample. The number of burst emissions was low and the level of continuous-type AE was again less than twice the background. The amplitude distribution of the burst emissions exhibited essentially a power-law behavior, with the slope of 1.5 to 2.3. The highest peak level observed was below 0.2 mV.

A typical AE behavior is shown in Fig. 2 for an S-sample, quenched and tempered at 450°C. Two distinct AE activities are indicated in the rms voltage-time curve. In the elastically loaded region, numerous spikes due to burst emissions are found, whereas a prominent peak is observed at the yield. The peak at the yielding is common to that observed in the L-sample of the same temper and consists of continuous-type emissions. The pre-yield, burst emission activities commenced at a very low load (at 1/6 of the yield load), and about 3000 events were recorded before reaching one-half the yield load. The amplitude distribution of the pre-yield burst emissions exhibited the characteristic Weibull distribution with an exponent of 0.3. The highest peak level exceeded 1 mV.

After tempering at higher temperatures, the continuous emission activities at the yield diminished along with the lowered yield strength. On the other hand, the pre-yield, burst emission activities became stronger. These trends, in effect, merged the two active regions into one. This is, in fact, the AE behavior of S-samples in the quenched and tempered or normalized and tempered at 650°C as well as in the as-received condition (2-7).

When an S-sample was slow-cooled after tempering treatment, the pre-yield burst emission increased up to 750°C tempering. On the other hand, the pre-yield burst activities started to diminish after 700°C tempering followed by quenching. Upon tempering at 750°C, the burst AE activities decreased to about 20% of these after 600°C tempering. This strong effect of cooling rate after tempering was essentially absent when S-samples were tempered at 650°C (7).

Effects of tempering temperature on the pre-yield, burst emissions can be seen most clearly in Fig. 3. Here, the AE event counts at 345 MPa (50 ksi) and at 413 MPa (60 ksi) are plotted against tempering temperature. These stress levels allow us to exclude the contribution of continuous AE signals. The AE event counts increased slightly after 150°C tempering, which could be discerned on the rms voltage vs. time curve as well. The burst activities increased several times after tempering at 250°C and 350°C, further increasing above the tempering temperature of 450°C to the levels of 4000 to 6000 event counts. The decrease in the burst activities in S-samples quenched after tempering is also shown in the figure, for the tempering temperature of 750°C in particular.

DISCUSSION

We have established by a series of studies on low-alloy steels that the pre-yield burst emissions (PYBE) are generated by the decohesion of MnS inclusions from the matrix (2-7). The PYBE were observed in the short transverse samples, but were absent in the longitudinal or transverse samples (5,6). These were proportional to the sulfur content. The steel had to be hot-rolled heavily to exhibit the PYBE; that is, MnS inclusions must be flattened so that tensile stress acts on their broad faces (4). Cooling speed from tempering treatment affected the stress at which PYBE were observed, indicating thermal stress has a role in the decohesion process (7). After PYBE were generated via tensile loading, these were recovered by additional heat treatments (11).

These findings, the last two in particular, have posed new questions as to the roles of thermal stress and heat treatment and possibly the diffusion of certain embrittling species, such as sulfur and phosphorous. Consequently, systematic tests have been conducted varying heat treatment. Among the present findings, we need to focus our attention on the following three points:

1. AE behavior was isotropic in the quenched samples and very limited numbers of burst emissions were observed, whereas the ductility parameters clearly showed that the S-sample is less ductile.

2. The PYBE increased with tempering temperature in the S-samples, but none was detected in the L-samples.

3. The PYBE started to diminish at tempering temperatures above 750°C when the sample was quenched, but remained active when slow-cooled.

These three points are interrelated, but we discuss them sequentially, leading to a plausible model that can explain the observed behavior.

In the quenched samples, burst emission activities were limited even in the S-samples. This can mean either the MnS-matrix interfaces are so strong that decohesion can occur under applied stress or almost all the interfaces have already been debonded prior to tensile testing and no further decohesion can take place during subsequent loading. For the former (strong interfaces), one may argue that any interfacial segregation is dispersed during austenitization because of the usual entropic effect (12) and that no impurity segregation is possible during quenching. It is further postulated that the interfaces without segregation can withstand high tensile stresses. This hypothesis cannot explain the ductility differential between the L- and S-orientations. The fracture surfaces of the two orientations were also distinctly different; the L-sample showing the radial shear ridges, while the S-sample exhibiting numerous MnS inclusions on the fracture surfaces. Figure 4 is the most deciding evidence against the strong interface hypothesis. This

is the fracture surface of a quenched s-sample, which revealed many more stringer-type MnS inclusions than those on the quenched and tempered samples with hundred times more AE event counts. This is a consequence of debonded interfaces; i.e., the second alternate hypothesis.

The debonded interface hypothesis is supported by the level of thermal stress, which develop at the MnS-matrix interface and within the inclusion itself. The thermal stress was calculated by Shibata and Ono (13) as the misfit stress, which is the principal component in comparison to the inhomogeneity effect or to the matrix deformation effect. Because of differential thermal expansion, tensile stress of 380 MPa develops at the interface (on the broad face). This result employed the temperature change during quenching of 900°C, the thickness-to-diameter ratio of an inclusion of 0.1, the Young's modulus of steel of 210 GPa and the thermal expansion coefficients of MnS and steel of 18.1 x 10^{-6}/°C and 12.5 x 10^{-6}/°C, respectively. The calculated thermal stress corresponds to that, below which most PYBE are observed in the as-received steel samples. Thus, it is likely that the interfaces are debonded during quenching. This is consistent with general observations that MnS is weakly bonded to the matrix (14). Most specifically, Brooksbank and Andrews (10) concluded, from their thermal expansion measurements of MnS and steel, that voids are created around MnS inclusions. They used precise lattice parameter measurements via X-ray diffraction to detect anomalous changes leading to the above conclusion.

It should be noted that the thermal stress is strongly dependent on the thickness-to-diameter ratio. For the ratio of 0.01, it decreases to about 50 MPa and for the ratio of 0.5, the stress is raised to 1200 MPa. Because of likely distributions in such ratios, the levels of thermal stress are expected to vary. The stress needed for debonding is another unknown. Since impurity segregation to grain boundaries is well-documented during austenitization, segregation to the interfaces may also be present, thus affecting the cohesive strength. An important point to note is that the debonding probably occurs during quenching. The temperature of debonding can possibly be as high as 300°-500°C.

Effects of tempering on the PYBE are demonstrated in Fig. 3. Additional experiments varying tempering time at 450, 550 and 650°C were performed. These showed almost immediate changes in the number of PYBE, followed by time dependent increases. That is, there are athermal and thermal components. Most PYBE below 350°C were due to athermal and the thermal components were less than 50% even at the tempering temperature of 650°C.

Since the preceding discussion has eliminated the strong interface hypothesis, we must consider mechanisms of bonding the separated surfaces of MnS and matrix. If the debonding occurs at temperature T, reheating above T will join the surfaces together. This should lead to mechanical (or physical) bonds, which can be strong because of the lack of contaminating atmosphere. This mode of bonding can rationalize the athermal component of the PYBE. Such bonding is further promoted as the inclusion generates compressive stress at the interface when temperature is raised above T.

The thermal component becomes significant above 450°C, suggesting a diffusional process. Two possible contributions are plausible. One is to complete the mechanical bonding processes mentioned above by supplementing local diffusion. This allows the development of chemically bonded interfaces. Since a stronger interface requires a higher mechanical force to debond, a more prominent PYBE is expected. Another mechanism relies on the impurity segregation. It has been well known that sulfur and phosphorous tend to segregate to free surfaces (15). This implies that impurity is likely to segregate to the debonded surfaces. The interfacial segregation is also plausible, especially when they are merely mechanically joined. The only

report indicative of such segregation has recently been made by Briant and Banerji (9). They examined a variously heat-treated Ni-Cr-Mn steel of high purity. Using Auger spectroscopy, they found that the interface has a 50% enrichment of S over the stoichiometric ratio of MnS. Such sulfur segregation at the interface can promote the bonding, but it is also likely that the interface is embrittled at lower temperatures. Both tendencies will contribute to the increase in the PYBE.

According to the above interpretation, one expects the thermal component to be controlled by the diffusion of sulfur to the interfaces. From the isothermal tempering data, we determined times, at which the thermal component started to increase. By plotting the times at three temperatures against the inverse absolute tempering temperatures, the activation energy of the thermal component was estimated to be 30 to 40 kcal/mole. While no diffusion data is available for sulfur in bcc iron, the data for fcc iron and that of phosphorous in bcc or fcc iron indicate that the diffusion of sulfur (or phosphorous) is involved during tempering.

The above discussion leads to two mechanisms; that is, mechanical bonding and impurity segregation to interfaces. These are the sources of increasing PYBE with tempering temperatures.

Finally, let us consider the decrease of PYBE above the tempering temperature of 700°C. This applies only when the S-samples were quenched after tempering. As was the case of the as-quenched condition, two mechanisms may be considered. One is the strong interface hypothesis, relying on the entropic effect to redistribute embrittling elements from the MnS-matrix interfaces. This parallels the usual interpretation of temper embrittlement. Once the interfaces are free of embrittling impurities, such as sulfur and phosphorous, the interfaces survive the thermal stress from quenching and remain intact even under applied stress. This hypothesis is difficult to test via the fractographic examination, because the PYBE still exist in substantial numbers (over 1000). Still we have found many MnS inclusions on the fracture surfaces. This finding tends to support the second hypothesis, although this is not a conclusive evidence. As before, the other mechanism relies on the weak or debonded interface hypothesis. Here, as the tempering temperature increases, the thermal stress also increases. Effects of quenching are minimal below 700°C, and the cohesive strength of the interfaces must be of the order of 300 MPa, which is the expected level of thermal stress. This value is comparable to the stresses which generate most PYBE. When an S-sample was slowly cooled from the 700-750°C range, the number of PYBE increased further to 10 to 15,000 counts from 4 to 6,000 after tempering at the 500-650°C range. Since the thermal stress is reduced substantially, this can be construed as a supporting evidence. However, the diffusion of embrittling species can proceed during the cooling. Thus, we cannot rule out the first hypothesis. Consequently, this part needs to be studied further to establish a convincing mechanism. To be consistent with the initial parts of this discussion, we tend to favor the debonding mechanism at this time.

Effects of heat-treatment on the PYBE can be schematically represented in Fig. 5. Upon quenching from the austenitization treatment, most inclusions are debonded. As shown in Fig. 5a, the number of bonded inclusions increases with tempering temperature. Initially, the bonding is a result of mechanical contact. Effects of diffusion are present at higher temperatures (above 400°C), producing chemical bonding as well. Thermal stresses causes the debonding in samples quenched after tempering above 700°C. Slow-cooled samples are not affected as severely, as shown in Fig. 5b. These factors combine to affect PYBE as shown in Fig. 5c, where the PYBE has a maximum when the samples were quenched after tempering. The PYBE for those with slow-cooling after tempering exhibits monotonic increase.

CONCLUSIONS

1. Pre-yield, burst emissions were detected in tempered A533B steel tensile samples of the short-transverse direction. These are due to the debonding of flattened MnS inclusions.

2. These burst emissions were absent in the longitudinal samples and in the as-quenched short-transverse samples. The burst emissions reappeared when the as-quenched short-transverse samples were tempered.

3. Thermal stress during quenching are responsible for the debonding of the MnS-matrix interfaces. The debonded interfaces contribute little to the generation of burst emissions.

4. During tempering, mechanical contact and impurity segregation to the interfaces re-establish the bonds between MnS and the matrix, unless debonded again by quenching after the tempering. These are responsible for the re-emergence of the burst emissions.

ACKNOWLEDGEMENTS

We are grateful for the support of this study by the Physics Program, the Office of Naval Research, and for the donation of the steel plate by Nippon Steel Corporation, Tokyo and Los Angeles.

REFERENCES

1. R.J. Landy and K. Ono, J. Acoust. Emission, 1 (1982) 7-19.

2. K. Ono and M. Yamamoto, Mat. Sci. Engr. 47 (1981) 247-263.

3. M. Yamamoto, C. Ouchi and K. Ono, Proc. 5th Int. Acoustic Emission Symposium, Jpn Soc. NDI, Tokyo, 1980, pp. 221-235.

4. K. Ono, R. Landy and C. Ouchi, Proc. 4th Acoustic Emission Symposium, International Technical Exchange Center, Tokyo, 1978, pp. 4-33 - 4-45.

5. K. Ono, H. Hatano and G. Huang, Proc. 8th World Conf. on Nondestructive Testing, Cannes, France, September 1976, Conference Secretariat, Paris, 1976, Section 3K, Paper 3K3, pp. 1-10.

6. K. Ono, G. Huang and A. Kawamoto, Internal Friction and Ultrasonic Attenuation in Solids, University of Tokyo Press, Tokyo, 1977, pp. 829-834.

7. K. Okajima and K. Ono, Proc. 5th Int. Acoustic Emission Symposium, Jpn Soc. NDI, Tokyo, 1980, pp. 270-281.

8. I. Roman and D. Jinchuk, Fatigue of Engineering Mat. Structures, 5 (1982), 71-76; I. Roman (to be published).

9. C.L. Briant and S.K. Banerji, Met. Trans. 13A, (1982), 827-836.

10. D. Brooksbank and K.W. Andrews, J. Iron Steel Inst., 206, (1968) 595-599.

11. I. Roman, K. Ono and H.B. Teoh, J. Acoust. Emission, 1 (1982) 71.

12. C.J. McMahon, Jr., "Temper Embrittlement in Steels," ASTM STP-407, Am.

Soc. Test. Mat., Philadelphia, 1967, pp. 127-167.

13. M. Shibata and K. Ono, Acta Met. 26 (1978) 921-932.

14. J.F. Knott, Metal Sci. 14 (1980) 327-336.

15. T. Takasugi, and D.P. Pope, Met. Trans. 13A (1982) 1471-81.

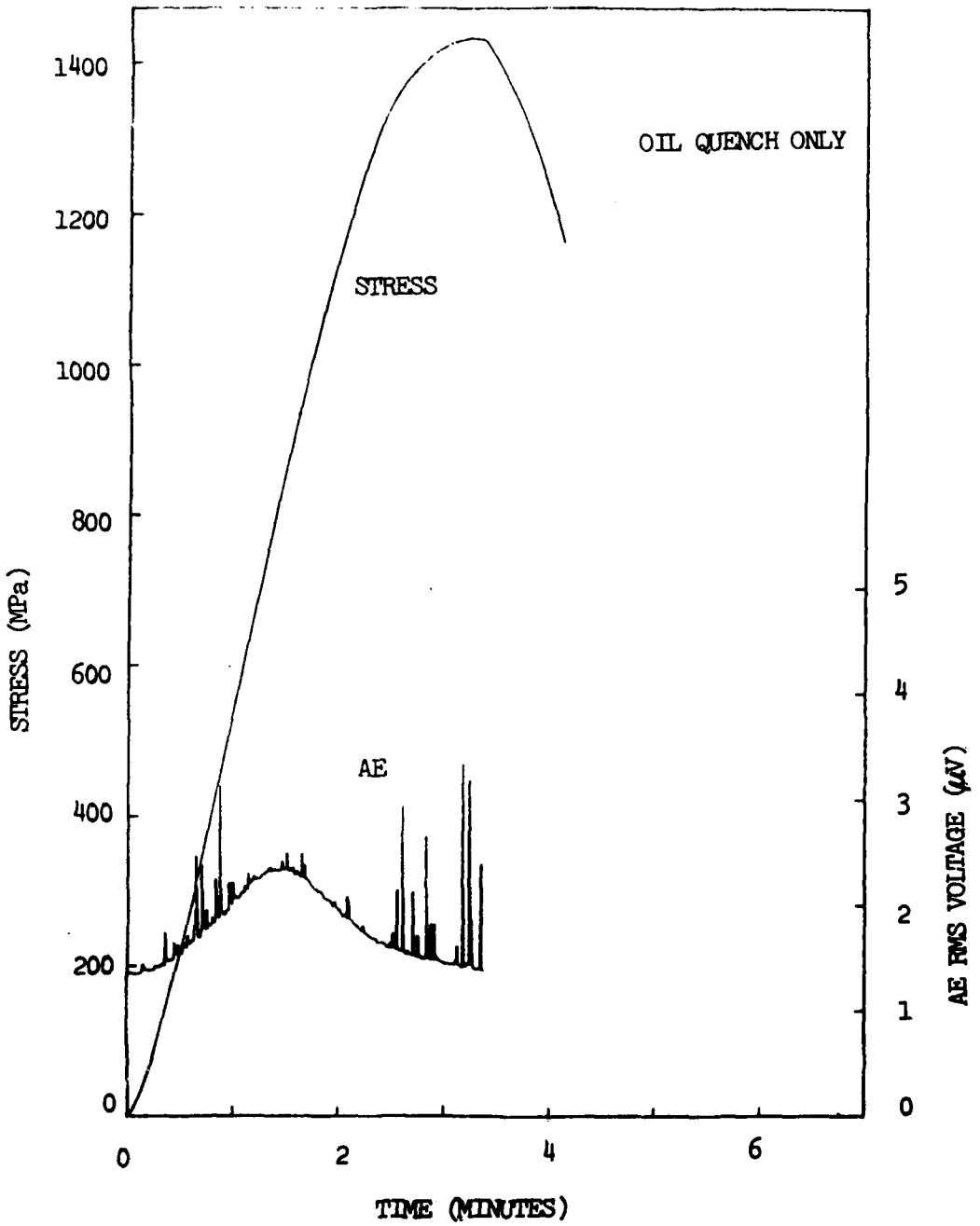

Fig. 1 Stress vs. time and rms voltage vs. time curves for an as-quenched longitudinal sample.

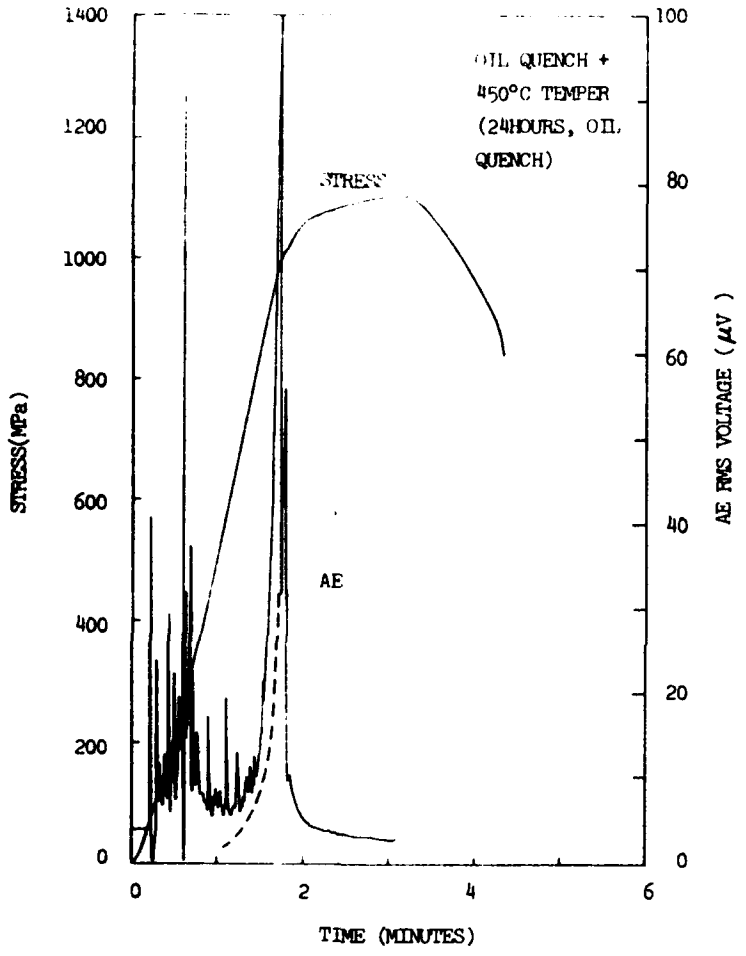

Fig. 2 Stress vs. time and rms voltage vs. time curves for a quenched and tempered short-transverse sample. The rms voltage curve below the yielding had 31.6 μV full scale.

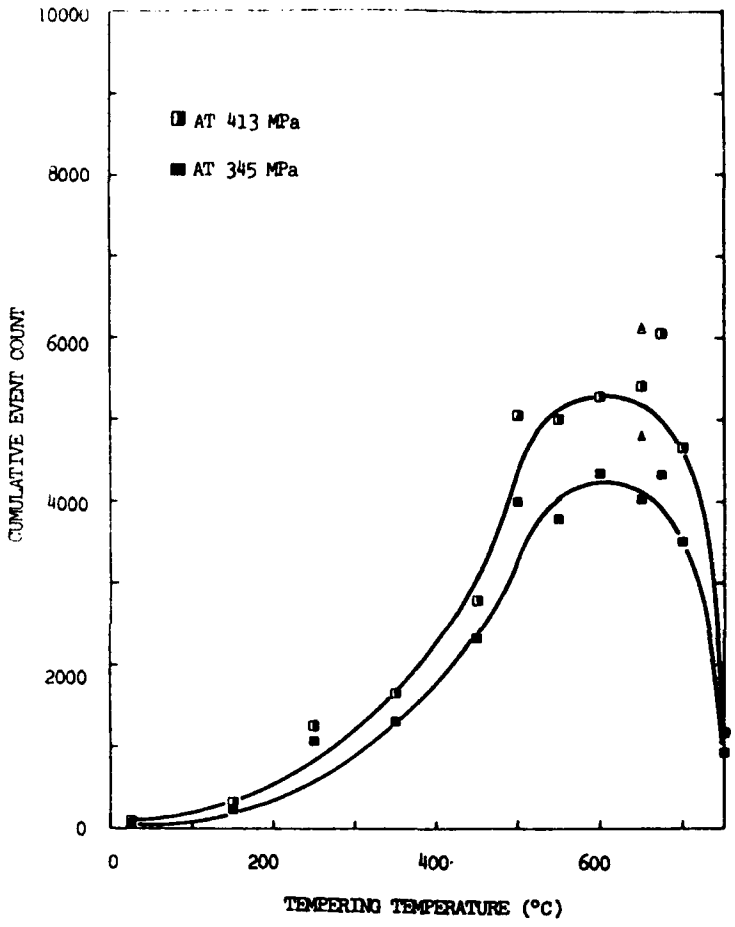

Fig. 3 Pre-yield, burst emission (cumulative) event counts vs. tempering temperature. Filled symbols are for event counts at 345 MPa and open symbols are for those at 413 MPa. Triangles represent the data from slow-cooled samples.

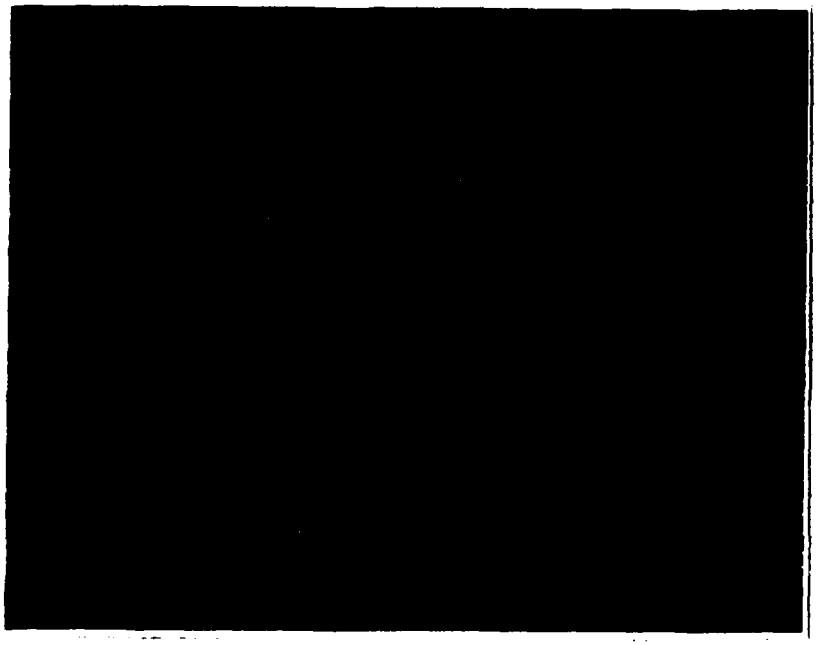

Fig. 4 Fracture surface of as-quenched, short-transverse sample, showing debonded MnS inclusions.

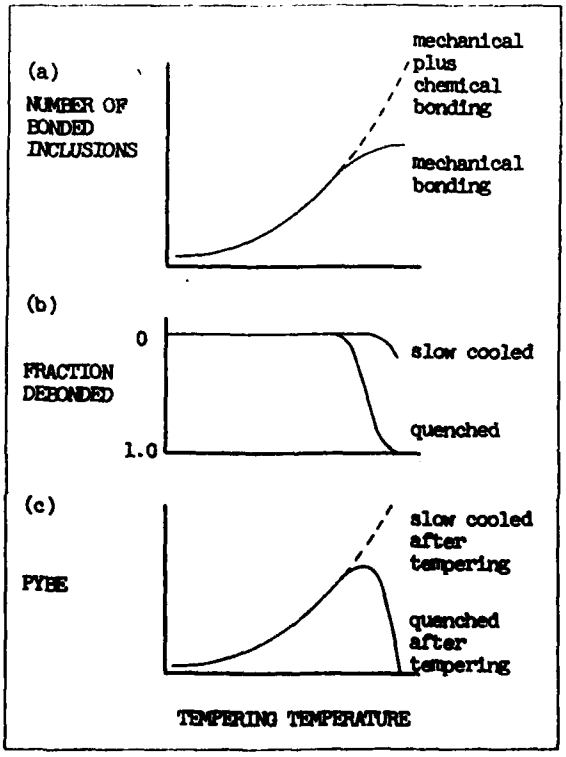

Fig. 5 Schematic chantes of the number of bonded inclusions (a), the fraction debonded by quenching (b) and the number of PYBE against tempering temperature.